



LUND UNIVERSITY

Systems level neurophysiological state characteristics for drug evaluation in an animal model of levodopa-induced dyskinesia.

Tamté, Martin; Brys, Ivani; Richter, Ulrike; Ivica, Nedjeljka; Halje, Pär; Petersson, Per

Published in:
Journal of Neurophysiology

DOI:
[10.1152/jn.00868.2015](https://doi.org/10.1152/jn.00868.2015)

2016

Document Version:
Peer reviewed version (aka post-print)

[Link to publication](#)

Citation for published version (APA):
Tamté, M., Brys, I., Richter, U., Ivica, N., Halje, P., & Petersson, P. (2016). Systems level neurophysiological state characteristics for drug evaluation in an animal model of levodopa-induced dyskinesia. *Journal of Neurophysiology*, 115(3), 1713-1729. <https://doi.org/10.1152/jn.00868.2015>

Total number of authors:
6

General rights

Unless other specific re-use rights are stated the following general rights apply:
Copyright and moral rights for the publications made accessible in the public portal are retained by the authors and/or other copyright owners and it is a condition of accessing publications that users recognise and abide by the legal requirements associated with these rights.

- Users may download and print one copy of any publication from the public portal for the purpose of private study or research.
- You may not further distribute the material or use it for any profit-making activity or commercial gain
- You may freely distribute the URL identifying the publication in the public portal

Read more about Creative commons licenses: <https://creativecommons.org/licenses/>

Take down policy

If you believe that this document breaches copyright please contact us providing details, and we will remove access to the work immediately and investigate your claim.

LUND UNIVERSITY

PO Box 117
221 00 Lund
+46 46-222 00 00

Systems level neurophysiological state characteristics for drug evaluation in an animal model of levodopa-induced dyskinesia

Martin Tamtè, Ivani Brys, Ulrike Richter, Nedjeljka Ivica, Pär Halje^a and Per Petersson^{a,*}

Integrative Neurophysiology and Neurotechnology, Neuronano Research Center, Department of Experimental Medical Sciences, Lund University, Medicon Village, Lund, Sweden

a) shared senior authorship

*) Corresponding author

Per Petersson

Medicon Village, Building 404 A2

Scheelevägen 2

223 81 Lund

Sweden

Per.Petersson@med.lu.se

Ph: +46 46 222 05 78

Fax: +46 46 275 60 11

Running Head: Systems level brain states

Abstract

Disorders affecting the central nervous system have proven particularly hard to treat and disappointingly few novel therapies have reached the clinics in the last decades. A better understanding of the physiological processes in the brain underlying various symptoms could therefore greatly improve the rate of progress in this field. We here show how systems level descriptions of different brain states reliably can be obtained through a newly developed method based on large-scale recordings in distributed neural networks encompassing several different brain structures. Using this technology we characterize the neurophysiological states associated with parkinsonism and levodopa-induced dyskinesia in a rodent model of Parkinson's disease together with pharmacological interventions aimed at reducing dyskinetic symptoms. Our results show that the obtained electrophysiological data add significant information to conventional behavioral evaluations and hereby elucidates the underlying effects of treatments in greater detail. Taken together, these results potentially open up for studies of neurophysiological mechanisms underlying symptoms in a wide range of neurologic and psychiatric conditions that until now have been very hard to investigate in animal models of disease.

Keywords: Systems neurophysiology, Parkinson's disease, Levodopa

Diseases affecting the central nervous system (CNS) are a rapidly growing concern that puts a great economic burden on society (Olesen et al., 2012) and cause major suffering for afflicted individuals and their families. Unfortunately, these diseases have also proven particularly hard to treat. In spite of the last decades' impressive advances in the field of molecular biology few novel therapeutic options have reached the clinics, notwithstanding recent corporate and regulatory efforts to break the trend (Graul, 2008). A major challenge in the development of new CNS therapies is the limited understanding of the basic processes governing normal brain functions, as well as the pathophysiological changes that ultimately cause the symptoms. For these reasons, the methodological approaches in drug discovery and development have often been limited to rather simplistic experimental read-outs. In pre-clinical studies, the evaluation of novel compounds typically involve characterization of changes in animal behavior in combination with *post mortem* tissue analyses with little information about the ongoing CNS changes causing the actual symptoms or the underlying physiological effects of an intervention. To make matters worse, several neurological and psychiatric conditions are not directly associated with overt changes in behavior, which makes them even more challenging to model in experimental animals. To gain an insight into such internal CNS processes, chronic electrophysiological recordings are a particularly promising approach which can give real-time access to neurophysiological activity patterns associated with physiological processes during natural conditions (Gervasoni et al., 2004; Lehew and Nicolelis, 2008). Building on this technology, large-scale sampling of neurophysiological signals from diverse brain regions could allow for the characterization of brain states that explains the difference between healthy and diseased states, as well as how these states are altered by drugs aimed at treating the disease. Though clearly a great experimental challenge, such detailed information on neurophysiological states obtained in valid animal models of CNS disease could significantly help to increase the rate of progress in research aimed towards new treatments for CNS disorders.

In fact, even recordings performed in single locations of the brain, such as those that have been obtained in Parkinson's disease (PD) patients implanted with electrodes in the subthalamic nucleus (STN) and the internal globus pallidus for the purpose of therapeutic deep-brain stimulation, have provided novel insights into pathological processes potentially underlying symptoms in this disease (Brown et al., 2001; Lalo et al., 2008; Brücke et al., 2012). In similar experiments on animals implanted with multiple electrodes, additional neurophysiological features have been identified that are thought to be associated with motor symptoms on and off medication. In particular, the parkinsonian hypokinetic state has been linked to an increased cell firing rate in the STN (Albin et al., 1989; Bergman et al., 1994; Levy et al., 2000), synchronized cell-firing in cortex (Goldberg et al., 2002), striatum (Goldberg et al., 2004), globus pallidus (GP; Nini et al., 1995) and STN (Bergman et al., 1994), as well as abnormally strong local field potential (LFP) oscillations in the beta band (~10-35 Hz) present across the entire cortico-basal ganglia network (Costa et al., 2006; Hammond et al., 2007; Fuentes et al., 2010; Stein and Bar-Gad, 2013). Dopamine replacement therapy alleviating parkinsonian symptoms has been shown to concomitantly suppress these aberrant activity patterns (Kreiss et al., 1997; Costa et al., 2006; Gilmour et al., 2011; Santana et al., 2014). Unfortunately, following long-term dopamine replacement therapy the therapeutic window frequently narrows to such an extent that treated subjects rapidly transition from parkinsonism to dyskinesia as the drug plasma concentration rises. In this situation, oscillatory activity in other parts of the LFP frequency spectrum has been reported to be markedly altered following levodopa administration in patients suffering from involuntary dyskinetic movements as a medication side-effect. Low-frequency oscillations in the theta range (4-10 Hz), for example, have attracted particular attention over the years (Alonso-Frech et al., 2006; Alegre et al., 2012; Alam et al., 2013), and more recently, characteristic gamma-oscillations (at ~ 80 Hz) in a rat model of PD were found to be strongly associated with levodopa-induced dyskinesia (Halje et al., 2012; Dupre et al., 2013). Equivalent high-

frequency oscillations have also been reported in STN-recordings in Parkinson patients, sometimes referred to as finely tuned high-gamma, but have in these studies primarily been thought to reflect the prokinetic state associated with the therapeutic effect of the medication (Cassidy et al., 2002; Brown, 2003; Sharott et al., 2005; Cagnan et al., 2014).

In order to clarify the association between different aberrant neuronal activity patterns and the expression of motor symptoms and to obtain a more comprehensive description of the neurophysiological state on a systems level, we have here made use of a technology developed in our lab that lets us perform large-scale multi-structure recordings in awake behaving rats (Fig. 1A, B; Ivica et al., 2014) in the most commonly used model of PD (the 6-OHDA lesioned rat; Nadjar et al., 2009). Applying this technology, we have investigated: 1) the neurophysiological state of the cortico-basal ganglia-thalamic circuit that is associated with parkinsonism, 2) the neurophysiological state that is associated with levodopa-induced dyskinesia and 3) the behavioral and electrophysiological effects of experimental and clinically used drug interventions aimed at alleviating dyskinetic symptoms.

METHODS

Animals

Four adult female Sprague Dawley rats (230–250 g) were used in the study. The animals were kept on a 12 h light cycle and received food and water *ad libitum*. All experiments were approved in advance by the Malmö/Lund ethical committee of animal experiments.

106

107 *6-Hydroxydopamine lesions and levodopa priming*

108 Rats were anesthetized with fentanyl/medetomidine (0.3/0.3 mg/kg, intra-peritoneal (i.p.)
109 injection) and fixed in a stereotaxic frame. The animals received two injections of 6-
110 hydroxydopamine (6-OHDA) hydrochloride (3.0 µg/µl free base dissolved in 0.02% ascorbate saline)
111 into the medial forebrain bundle of the right hemisphere at the following coordinates from bregma
112 and cortical surface (Lundblad et al., 2002): Injection site (I), 2.5 µl: tooth bar (TB): -2.3;
113 anteroposterior (AP): -4.4; mediolateral (ML): -1.2; and dorsoventral (DV): -7.8; Injection site (II), 2.0
114 µl: TB: +3.4; AP: -4.0; ML: -0.8; DV: -8.0. Moderate motor impairments including asymmetric posture
115 and gait and reduced contralateral forelimb dexterity were generally apparent two weeks after
116 lesioning. One week after lesioning animals were given daily doses of levodopa (6mg/kg) for two
117 weeks. After two weeks of treatment, the animals that showed moderate to high levels of dyskinetic
118 symptoms after having been challenged with 12mg/kg levodopa were implanted and included in the
119 study.

120

121 *Implantation surgery*

122 Implantations were performed under fentanyl/medetomidine anesthesia (0.3/0.3 mg/kg, i.p.) at
123 least three weeks after 6-OHDA lesions. Microwire electrodes were implanted in both hemispheres.
124 The eight regions targeted in each hemisphere were: Rostral Forelimb Area (RFA - a rodent
125 supplementary motor area), primary motor cortex (MI), dorsolateral striatum (DLS), dorsomedial
126 striatum (DMS), globus pallidus (GP), ventrolateral/ventroanterior nuclei of the thalamus (VL/VA;
127 projecting to motor cortex), subthalamic nucleus (STN) and substantia nigra pars reticulata (SNr).
128 Center coordinates in relation to bregma and the cortical surface were in the following structures:

RFA, AP: +3.75, ML: ± 2.0 , DV: -1 (Neafsey and Sievert, 1982); MI, AP: +1.5, ML: ± 2.8 , DV: -1.0 (Gioanni and Lamarche, 1985); the DLS, AP: +0.2, ML: ± 3.8 , DV: -4 and DMS, AP: +0.2, ML: ± 2.8 , DV: -4, (West *et al*, 1990); GP, AP: -1.0, ML: ± 3 , DV: -5.5-7.2 (Chen *et al*, 2011); VL/VA, AP: -2.6, ML: ± 1.75 , DV: -6.5 (Paxinos and Watson, 2007); STN, AP: -3.5, ML: ± 2.3 , DV: -7.5-8.2 (Tai *et al*, 2003); SNr, AP: -5.4, ML: ± 2.4 , DV: -7.8-8.8 (Wang *et al*, 2010). The implant was fixated with dental acrylic, which was attached to screws in the skull. After surgery, the anesthesia was reversed by atipamezole hydrochloride (5 mg/kg, i.p.) and buprenorphine (0.5 mg/kg, subcutaneous (s.c.) injection) was administered as postoperative analgesic. The animals were allowed to recover for one week after surgery before testing commenced.

Experimental procedure

During recording sessions animals were placed in a transparent cylinder (250 mm in diameter), and their behavior was recorded with digital video in parallel with the electrophysiological recordings (synchronized via an external pulse generator; Master-8, AMPI). The same paradigm was used in each experiment: First, the rat was recorded for ~ 30 min to establish baseline conditions. Second, the rat received an i.p. injection with 12mg/kg levodopa (levodopa methyl ester hydrochloride) and 12mg/kg benzerazide (serine 2-(2,3,4-trihydroxybenzyl) hydrazide hydrochloride). The time point of this injection marks the beginning of the experimental timeline, i.e., $t = 0$ min. Dyskinesia developed 10 to 20 min post-levodopa injection and reached its peak severity ~ 60 min post-levodopa injection. In experiments not involving further pharmacological intervention, the recordings continued until the dyskinesia diminished spontaneously (~ 2 -3 h after dyskinesia onset). Experiments involving additional drug treatment are described below.

Pharmacology

Following levodopa injection and the manifestation of dyskinesia a number of pharmacological substances were evaluated with respect to their anti-dyskinetic effects. Injection time points were chosen such that each drug would exhibit its therapeutic effect during the time of peak dyskinesia. Once the pharmacological effect of the serotonin 5-HT_{1A} receptor agonist 8-OH-DPAT (1 mg/kg & 0.4 mg/kg i.p., t = ~60 min) had been established the specificity of the intervention was verified by injection of the 5-HT_{1A} antagonist WAY-100,635 (0.5 mg/kg & 0.4 mg/kg i.p., t = ~100 min), which effectively reversed the effect of 8-OH-DPAT. The neurophysiological and behavioral effects of the clinically used anti-dyskinetic drugs amantadine hydrochloride (a NMDA receptor antagonist, 50 mg/kg & 50 mg/kg i.p., t = ~60 min), diazepam (a positive allosteric modulator at GABA_A receptors, 5 mg/kg i.p., t = ~60 min) and levetiracetam (a pre-synaptic calcium channel inhibitor, 80 mg/kg & 120 mg/kg i.p., t = ~30 min) were also evaluated. All drugs used in this study were attained from Sigma Aldrich, Sweden and doses were chosen according to previously published studies (Kannari et al. 2001; Peixoto et al. 2005; Tronci et al. 2014; Coppola et al. 2010).

Assessment of dyskinesia severity

The scoring of dyskinesia was performed offline, using an adapted version of the scoring methods of abnormal involuntary movements (AIMs) described by Cenci and colleagues (Lundblad et al., 2002). In summary, three different types of AIMs (orolingual, forelimb, and axial dyskinesia) were scored with respect to their severity for monitoring periods of 1 min with 5-minute intervals. In addition, contraversive rotations with respect to the lesioned side were also quantified, as rotational behavior is correlated with general dyskinetic symptoms in this model (Breger et al., 2013). Forelimb and axial AIMs and rotations were rated on a scale ranging from zero to three where zero equals no

dyskinesia and three equals continuous dyskinesia. Orolingual dyskinesia was less clearly detectable in the videos and was therefore scored as one when detected and zero otherwise. The measures for all AIMs and rotations were normalized per category [0, 1] and then added together to produce a total AIM value [0, 4] for each assessed 1-minute period. This combined value was taken to indicate the overall severity of the dyskinesia at any given time.

Recording electrodes

For details on electrode design see (Ivica *et al*, 2014). In brief, formvar-insulated tungsten wires (33 μm) were arranged into sixteen groups of arrays (eight per hemisphere; Fig. 1A) with 250 μm wire spacing in each horizontal dimension and fixed to the length corresponding to the implantation site for each group. Each array consisted of a minimum of five recording channels and one reference channel. All wires were connected to a custom made printed circuit board and linked via connectors/adaptors to the pre-amplifier of the acquisition system. A 200 μm thick silver wire was attached to the skull screws and used as a ground connection from the animal to the recording system.

Signal acquisition

Neuronal activity was recorded with the Neuralynx multichannel recording system using a unity gain pre-amplifier (HS-36, Neuralynx, MT, USA). LFP signals were filtered between 0.1 and 300 Hz, and were digitized at 1017 Hz. Unit activities were filtered between 600 and 9000 Hz, and were digitized at 32 kHz. Thresholds for storage of spiking events in each channel was automatically set to three SDs of the unfiltered signal.

197

198 *Spike sorting*

199 Action potentials were sorted manually into unit clusters using Offline Sorter (Plexon Inc.).
200 Waveform features used for separating the units were, e.g., valley and peak amplitude or the first
201 three principal components of all the 32-element vectors defining the sampled waveforms for a given
202 dataset. A cluster was classified as single unit (SU) when less than 0.1 % of the spikes in a defined
203 cluster occurred within the refractory period (set to 1.6 ms), and as multiunit otherwise (Harris *et al*,
204 2000).

205

206 *Frequency analysis of LFPs*

207 To emphasize local sources of the measured electrical potential (and to minimize effects of
208 the choice of amplifier reference), bipolar LFP time series were computed offline from all unique
209 pairs of electrodes from the same structure. For each of these time series, time-frequency
210 spectrograms were calculated over the entire frequency range with a multitaper method (Pesaran,
211 2008) (50%-overlapping 8-s windows, time-bandwidth product 4, 7 tapers) implemented in Chronux
212 2.0 (Mitra and Bokil, 2008). Power line noise (50 ± 2 Hz and 1st harmonic at 100 ± 2 Hz) was removed
213 from the power spectral densities (PSDs). To better identify oscillations in certain part of the
214 frequency spectrum, each individual power spectrum was normalized to the pink noise background.
215 That is, the noise background was estimated once for each 8-s window and for each bipolar channel
216 separately. Due to the complexity of the data it was not possible to manually pick enough frequency
217 bands with pure pink noise in all structures and conditions to get unbiased estimates of the noise
218 background. Instead we divided the whole frequency axis (from 1 to 200 Hz) into 20 logarithmically
219 spaced bands (1-1.3, 1.3-1.7, ..., 151.3-200) and used the median power of each band for the fitting

of the pink noise power curve $S(f)=b/f^a$. The pink noise normalization allowed us to describe deviations from the pink noise floor in terms of the unit dB_{pink} , defined as

$$S_{dB(\text{pink})}(f) = 10\log_{10} \frac{S(f)}{S_{\text{pink}}(f)}$$

where $S(f)$ and $S_{\text{pink}}(f)$ have the dimension power per frequency (i.e. V^2/Hz) and $S_{dB(\text{pink})}$ is expressed in the dimensionless unit dB_{pink} .

As a final step, an average spectrogram was calculated for each structure, based on the pink noise corrected spectrograms for each individual local bipolar LFP time series.

In Figs. 2-4 and 7, the obtained spectrograms were further averaged over time for each behaviorally classified state in order to obtain average spectra for the different states.

Systems level neurophysiological states

In order to visualize and identify systems level neurophysiological states we relied on the average, pink-noise normalized spectrograms that were calculated for each structure in each recording session, as described above. Each such spectrogram consists of a series of individual spectra reflecting the frequency content between 2 and 120 Hz with 0.5 Hz resolution in that structure during an 8-s window. The electrophysiological samples (made up of 8-s recording segments) included from each state were selected from within a time interval during a steady state, as defined by behavioral criteria (dyskinesia score; see Table 1A for a summary of the number of samples obtained in each animal and state). Samples were defined, such that one sample contained the concatenated spectra from all structures for one such 8-s window. Thus, for one recording session the number of samples n becomes equal to the number of 8-s windows, and the number of variables p becomes equal to the number of frequency bins (2 x the frequency range) times the number of structures. Pooling all recording sessions in one animal results in a number of samples n_{pooled} equal to

the number of 8-s windows in all these recording sessions, while the number of variables p stays the same.

A first aim was to obtain a two-dimensional visualization of the samples describing the spectral differences to the control state along the axes <Control vs. PD> and <Control vs. Dyskinesia>. The following steps have been taken: The data is normalized such that the mean and standard deviation over each variable become zero and one, respectively. The samples normalized in this way are denoted by \mathbf{s}_i , $i = 1, \dots, n$. Next, the origin of the coordinate system is shifted to become equal to the cluster center of the control state, i.e., the mean over all samples belonging to the control state, $\bar{\mathbf{s}}_{control}$, is subtracted from each sample: $\tilde{\mathbf{s}}_i = \mathbf{s}_i - \bar{\mathbf{s}}_{control}$. By this, each shifted sample $\tilde{\mathbf{s}}_i$ describe the spectral differences to the mean control state. In order to obtain a two-dimensional representation of the data, an x- and y-axis are defined to point from the cluster center of the control state, i.e., the origin of the shifted coordinate system, to the PD and dyskinesia cluster center, $\bar{\mathbf{s}}_{PD}$ and $\bar{\mathbf{s}}_{dys}$, respectively. However, for the y-axis its projection on an axis orthogonal to the x-axis will be shown. The projection onto the x- and y-axis is furthermore normalized such that the PD and dyskinesia cluster centers will have an x- and y-value equal to zero and one, respectively. Mathematically, the value on the x-axis for the shifted sample $\tilde{\mathbf{s}}_i$ can be obtained from

$$x_i = \tilde{\mathbf{s}}_i \cdot \frac{\bar{\mathbf{s}}_{PD}}{\|\bar{\mathbf{s}}_{PD}\|_2^2} ,$$

and the value on the orthogonal y-axis can be obtained from

$$y_i^{ortho} = \tilde{\mathbf{s}}_i \cdot \frac{\bar{\mathbf{s}}_{dys}^{ortho}}{\|\bar{\mathbf{s}}_{dys}^{ortho}\|_2^2} \text{ with}$$

$$\bar{\mathbf{s}}_{dys}^{ortho} = \bar{\mathbf{s}}_{dys} - \frac{\bar{\mathbf{s}}_{PD} \cdot \bar{\mathbf{s}}_{dys}}{\|\bar{\mathbf{s}}_{PD}\|_2^2} \bar{\mathbf{s}}_{PD} ,$$

where \cdot denotes the dot-product, and $\|\cdot\|_2$ denotes the L2-norm. Figures 3A (and 9D) show the results of this visualization. Furthermore, in Fig. 3B the vectors $\tilde{\mathbf{s}}_{PD}$ and $\tilde{\mathbf{s}}_{dys}^{ortho}$ are illustrated, while Fig. 7D illustrates the eight structure components that makes up the vector $\tilde{\mathbf{s}}_{8-OH-DPAT}$ (i.e., the cluster center of the 8-OH-DPAT treatment state in the shifted coordinate system). Finally, for Figs. 3C,D and 9 the above analysis has been performed for each structure separately (i.e., without concatenating the spectra from all structures), and the distributions of x_i for the control and the PD cluster are shown in Fig. 3C, while Fig. 3D shows the distributions of y for the control and the dyskinetic cluster. Note that we chose to not use y_i^{ortho} in Fig. 3D, but rather the more intuitive distribution defined by

$$y_i = \tilde{\mathbf{s}}_i \cdot \frac{\tilde{\mathbf{s}}_{dys}}{\|\tilde{\mathbf{s}}_{dys}\|_2^2},$$

which exclusively depends on the difference between the control and the dyskinetic states.

Quantification of state separability

To quantify the separation between states in terms of classification performance it was necessary to first reduce the dimensionality of the data using principal component analysis (PCA). We used the singular value decomposition PCA algorithm with variance weighting (Matlab). Generally speaking, given a dataset with n samples and p variables, all samples can be represented in a p -dimensional coordinate system. PCA can be thought of performing a high-dimensional rotation of this coordinate system according to

$$\mathbf{T} = \mathbf{S}\mathbf{W},$$

where \mathbf{S} and \mathbf{T} are $n \times p$ matrices representing the samples in the original and the rotated coordinate system, respectively, and \mathbf{W} is the $p \times p$ rotation or weight matrix. In PCA, the weight matrix \mathbf{W} is constructed such that the p variables in the new coordinate system are uncorrelated over the dataset. Furthermore, the first variable in this coordinate system, i.e., the first principal component, will by definition capture the most variance of the dataset, the second principal component will capture the second-most variance in a perpendicular dimension to the first, and so forth. Thus, would one only keep the first two principal components, one would automatically obtain a representation of the dataset in the two-dimensional plane in which the data is most spread out, allowing a convenient visualization of the high-dimensional data and, e.g., the identification of clusters. For example, in Figure 9B the first three principal components, obtained from applying PCA to the pooled data in one animal, are shown. Such a visualization can complement visualizations based on the method described in the previous section, where differences between selected states are emphasized by projection onto the state difference vector.

After dimensionality reduction with PCA a Gaussian mixture model was fitted to the data (Matlab fitgmdist function). The number of Gaussian components in the model was set to be equal to the number of experimental conditions (e.g. control, control+levodopa, PD and Dyskinesia) and the starting conditions for the optimization (means, covariances and mixing proportions) were calculated by assigning samples from the same experimental condition to one Gaussian component. The performance of the model was then estimated by assigning each sample to the Gaussian component with the largest posterior probability (weighted by the component probability) and calculating the average number of correct classifications. Generally, the classification performance improved as more principal components were added, until a plateau was reached (c.f. Fig. 10). Chance level of correctly assigning a data point to one of n states corresponds to $p = 1/n$. As a compromise

between the risk of over-compressing the data and the cost of performing heavy calculations we settled on consistently using 30 principal components for all quantifications of classification performance.

To complement classification performance as a measure of state separability, classical frequentist hypothesis tests were performed to test for significant differences between states. For each possible state pair the data was projected orthogonally onto a line going through the means of the two distributions, i.e. for example the line defined by the vector $\bar{s}_{PD} - \bar{s}_{dys}$. The distributions (now 1-dimensional) were then tested with a standard Wilcoxon rank sum test corrected for multiple comparisons (Bonferroni).

Tissue preparation and immunostaining

Animals were anesthetized with a lethal dose of sodium pentobarbital (100mg/kg) and heads were fixated in 4% paraformaldehyde. Brains were removed, post fixed in paraformaldehyde overnight and then transferred to 30% sucrose PBS (phosphate-buffered saline) solution at 4°C overnight for cryoprotection. Using a cryostat, tissue was sectioned in 50 µm thick coronal slices and mounted on charged slides. The placement of electrodes was verified in coronal brain sections stained with cresyl violet in two animals. The extent of the lesions was confirmed by tyrosine hydroxylase (TH) immunohistochemistry.

Cresyl violet staining

Sections were stained with 0.1% cresyl violet (CV) powder in dH₂O and 0.3% glacial acetic acid solution for 5 min. Sections were then rinsed for 1 min in dH₂O and dehydrated with 70%, 95%

and 99.5 % EtOH for 1 min each and then immersed in 100% xylene for 5 min (x2) before mounted with DPX mounting media.

Tyrosine Hydroxylase (TH) staining and quantification

Brain sections were washed in PB 0.01M (5 min), hydrogen peroxide 0.3% diluted in methanol (20 min), PBS/Tween 0.05% (5 min) and then were incubated in 10% normal goat serum for 30 min, followed by incubation with primary antibody rabbit anti-TH (1:500, Chemicon) overnight at room temperature. On the following day, sections were rinsed in PBS/Tween 0.05% (5 min) and incubated with biotinylated goat anti-rabbit (1:200, Vector) for 2 hrs. After that, all sections were rinsed in PBS/Tween 0.05%, incubated in avidin-biotin complex (ABC Kit, Vector) for 1 hr and stained with 3,3-diaminobenzidine and H₂O₂.

TH striatal optical densitometry was assessed using the ImageJ software (National Institutes of Health) as described previously (Fuentes *et al*, 2009) in areas adjacent to the striatal recording sites. The optical density of the ipsilateral corpus callosum was used as staining background and was subtracted from striatal values prior to comparison.

Statistical methods

All statistical tests used to assess significant group difference are specified in the Result section of the main text and in the respective figure legends.

RESULTS

Experiments performed

To clarify which neurophysiological activity patterns are associated with parkinsonism and dyskinetic states in PD we performed parallel multi-structure neuronal recordings in eight different parts of the cortico-basal ganglia-thalamic loop using the described novel methodology. In total, 15 separate recording sessions were performed in four unilaterally 6-OHDA lesioned dyskinetic rats (repeatability was evaluated by performing nine separate recordings in the same subject in experiments performed several weeks apart and reproducibility by performing similar recordings in four different subjects). *Post mortem* TH staining adjacent to the recording electrodes showed a complete loss (100%) of dopaminergic terminals in posterior parts of the striatum ipsilateral to the lesion with some remaining terminals in anterior areas (average striatal denervation ~74%). In seven of these experiments additional pharmacological interventions aimed at reducing dyskinetic symptoms were also investigated as a proof-of-principle for the use of the developed technology in characterization of experimental treatment of disease.

Recordings in STN/M1 confirm previously reported changes in neuronal activity patterns

From the obtained recordings, we could confirm the presence of narrow-band high-frequency gamma oscillations in M1 (as previously documented in rodents) and theta-oscillations in STN (as previously documented in humans) after the transition from the parkinsonian to the dyskinetic condition following levodopa treatment (Fig. 2A, B; Alonso-Frech et al., 2006; Halje et al., 2012). A notable difference between these two phenomena was however that narrow-band gamma-oscillations at no instance were observed in neither the intact hemisphere during dyskinesia nor the lesioned hemisphere of non-levodopa treated animals, as opposed to theta oscillations that were more abundantly present (in particular during periods of increased motor activity). From the spectrograms presented in Fig. 2A, it is clear that the spectral contents in the parkinsonian condition

varies over time (examinations of the video recordings revealed that these changes were associated with changes in behavioral state of the animal, in agreement with previous studies (Avila et al., 2010; Brazhnik et al., 2014; Delaville et al., 2014)). In contrast, following a transient frequency-tuning at the onset of dyskinesia, the spectral characteristics in the dyskinetic state was relatively stable throughout the dyskinetic period.

Within an individual the theta/gamma power changes in STN/M1 were consistent across recordings (average power spectra from nine example recordings from the animal shown in Fig. 2A are presented in Fig. 2B). On the other hand, between rats, peak frequencies within the different bands were found to vary somewhat. On average over all the recordings, there was an increase in LFP power for the theta band [3-9 Hz] when comparing the dyskinetic state to the baseline prior to levodopa administration (Wilcoxon signed rank tests revealed that the 1.9 dB increase in STN was significant ($p=0.0004$), while the 0.3 dB increase in M1 was weakly significant ($p=0.05$) and did not survive correction for multiple comparisons). For the gamma band [65-100 Hz] a significant increase was only found in M1 (Wilcoxon signed rank tests revealed +0.1 dB, $p=0.4$, for STN and +3.0 dB, $p=0.0004$, for M1). In this context it is also interesting to note that a comparison to the levodopa treated control side revealed that the theta increase following levodopa administration may partly be related to the induced increase in motor activity in contrast to the changes in gamma which are more specific to the dyskinetic state. Wilcoxon signed rank test for differences in the increase of power in the theta band between the STN in the two hemispheres before and after treatment, showed that the side difference was not quite significant ($p=0.054$, after Bonferroni correction for multiple comparisons [$n=4$]). For the gamma band, on the other hand, the corresponding power increase in M1 after treatment was significantly higher in the lesioned hemisphere compared to control ($p=0.0032$).

396

397 *Multi-structure recordings reveal systems level brain states*

398 Based on these confirmatory findings in M1 and STN, it is expected that abnormal activity
399 patterns should arise under similar conditions also in other parts of the highly interconnected circuits
400 making up the cortico-basal ganglia-thalamic loop. Moreover, although these specific frequency-
401 bands which have been highlighted in earlier studies indeed showed clear changes in relation to the
402 transition from parkinsonian to dyskinetic state, it is evident that other parts of the frequency
403 spectrum also displayed changes (which appeared to differ between M1 and STN; Fig. 2A, B). In the
404 subsequent analyses we therefore included all simultaneously recorded structures from both
405 hemispheres and did not restrict LFP-analyses to delimited frequency bands. Recordings from four
406 different conditions were analyzed: 1) from the intact hemisphere OFF-levodopa, representing the
407 control condition, 2) from the lesioned hemisphere OFF-levodopa, representing the parkinsonian
408 state, 3) from the lesioned hemisphere ON-levodopa during periods with dyskinesia, representing the
409 dyskinetic state, and 4) from the intact hemisphere ON-levodopa, representing a second control
410 condition in the drug-treated state. Recordings from these different conditions were divided into
411 separate data sets and analyzed individually for each rat. LFPs and the firing rates of individual
412 neurons were both examined. For LFPs, frequency power spectra (based on the spectral contents
413 between 2 and 120 Hz with a 0.5 Hz resolution) were calculated during 8-s sample periods for all
414 brain structures. To describe the neurophysiological state of an animal at different time points during
415 the experiment the power spectra from the different structures were combined into a single vector,
416 thereby essentially creating a unique coordinate in this high-dimensional space for each 8-s time bin.
417 Similarly, for firing rates, the neurophysiological state was also described by a unique coordinate for

each 8-s period created from the vector comprising the average firing rate of all recorded neurons during each sample period.

In all recorded experiments, behavioral observations confirmed that animals quickly transitioned into a stable severely dyskinetic state following levodopa treatment and remained in this condition with uninterrupted dyskinesia for an average time period of 160 ± 22 min (corresponding to the reported period of elevated levodopa concentrations Carta et al., 2006) unless other pharmacological interventions were carried out. This was expected given that medial forebrain bundle lesions are known to cause a severe model of PD where practically no therapeutic window for dopamine replacement therapy remains following a brief period of levodopa treatment (Winkler et al., 2002). When pooling LFP data from parkinsonian and dyskinetic animals from multiple recordings and plotting the coordinates in a 2D-space chosen to facilitate the comparison of the two pathological states (i.e. where the x-axis represents the difference vector between the parkinsonian and control state and the y-axis the difference vector between the dyskinetic and control state in the direction orthogonal to the x-axis) it became obvious that data sampled from time periods belonging to each specific state clustered in separate parts of the plane (Fig. 3A). Moreover, this LFP-based state description proved to be very robust across experiments performed in each animal (denoted by filled triangles in Fig. 3A; see Table 1B for details on state classification performance).

To get a better understanding of the underlying physiological differences separating the states, the spectral content in each structure was analyzed in further detail. In Fig. 3B the mean of the spectral differences that chiefly separate the control from the parkinsonian state and the dyskinetic from the control state in Fig. 3A (i.e. the axes spanning the plane) is plotted for all eight brain structures in Animal I, which has the largest number of recordings. Note the increase in relative LFP-power in the beta band in several structures in the parkinsonian state, as well as the theta and

gamma-peaks in the dyskinetic state (Fig. 3B top and bottom, respectively). However, certain variability between subjects in terms of the exact difference spectra that separate the states were also observed (Fig. 4). These inter-individual differences could be expected given inherent variability between individuals relating to brain circuit anatomy, the exact locations of the recording electrodes, signal-to-noise levels etc. On the other hand, the great similarities in the state representations (Fig. 3A) show that comparisons of similar states across subjects can be made even though the absolute differences between states in terms of LFP spectral contents may vary between individuals.

To investigate the relative contribution from the eight different brain structures for state separation we also analyzed state classifications based on the LFPs recorded in each single structure (for details on calculations see Methods). In Fig. 3C the state separations [Control vs. PD] and [Control vs. Dyskinesia] obtained for each structure are shown separately. These analyses show that the LFP spectral contents in e.g. cortex and STN constitute relatively reliable biomarkers for these three states (see also Halje et al., 2012). Nonetheless, state separation for any individual structure was clearly not as robust as the multi-structure data – for example, whereas the average classification performance for all recordings was 98.6% using data from all structures it was reduced to 85.6% when using data from M1 and STN only, (cf. Fig. 2B), which corresponds to a >10-fold higher error rate than when all eight structures are included (histograms for all animals are included in Fig. 5 and classification performance in Table 1B).

We next analyzed changes in neuronal activity. Here, the requirement of sampling unit activity from the same neurons across states limits comparisons to changes observed within each structure across different experimental conditions. Hence, in the unilateral 6-OHDA PD-model direct comparisons between the control and the parkinsonian/dyskinetic state cannot be obtained with single-cell resolution. Even so, when analyzing unit activity of cells located in the lesioned

hemisphere we found that several neurons clearly altered their firing rates during dyskinesia compared to the parkinsonian state (increased: RFA 2/6, DMS 7/10, DLS 6/11, GP 0/9, Thal 9/9, STN 2/9; decreased: RFA 3/6, DMS 3/10, DLS 3/11, GP 9/9, Thal 0/9, STN 5/9; $p < 0.05$, Wilcoxon rank sum test). Consequently, these two states could be reliably separated in a similar manner to the LFP-based clustering (in the corresponding multi-variate analysis across the two states, i.e. ON/OFF levodopa). See Fig. 6 for example state plots based on unit data (average classification performance for PD vs. dyskinesia was in this case 99.3%).

Ameliorating dyskinetic symptoms using a serotonin agonist

For the vast majority of Parkinson patients, dopamine replacement therapy effectively improves a range of symptoms and remains the therapeutic approach of choice (PD MED Collaborative Group, 2014). The possibility to prolong the levodopa treatment period before complications arise, by reducing drug-induced dyskinetic symptoms has therefore attracted a lot of interest in recent years (Olanow et al., 2000; Crosby et al., 2003; Huot et al., 2013). One such approach is the use of serotonin (5-HT) agonists aiming to control the efflux of dopamine from serotonergic terminals of dorsal raphe neurons by stimulation of 5-HT auto-receptors (Carta et al., 2007; Svenningsson et al., 2015). The rationale for this method stems from the notion that dyskinesia is partly caused by a dysregulation in dopaminergic signaling and that serotonergic terminals synthesizing dopamine via Aromatic L-amino Acid Decarboxylation (AADC) release it in an uncontrolled manner (the AADC-enzyme is in serotonergic neurons responsible for the synthesis of 5-HT but can also convert levodopa into dopamine). Accordingly, a pharmacological intervention targeting presynaptic 5-HT receptors on these neurons could potentially harness the uncontrolled synaptic release of dopamine. To evaluate the potential of this approach from a systems level point

of view, we first administered the 5-HT_{1A} agonist 8-OH-DPAT systemically during peak dyskinesia and subsequently reversed the effect of the drug by treatment with the 5-HT_{1A} antagonist WAY-100,635 ~40 minutes later. Dyskinetic symptoms were quantified during different phases of the experiment with respect to prevalence of the abnormal involuntary movements observed (Lundblad et al., 2002).

The 5-HT_{1A} agonist was found to effectively ameliorate dyskinesia and this effect was fully reversible by the antagonist (Fig. 7A; mean normalized scores [0, 1]: Dyskinesia=0.72, 8-OH-DPAT=0.01, WAY100635=0.75; Kruskal-Wallis $p<0.001$, Dunn's post-test for group differences: Dys vs. 8-OH-DPAT, $p<0.01$; 8-OH-DPAT vs. WAY100635, $p<0.001$; Dys vs. WAY100635, n.s. based on dyskinesia scores >5 min after each injection [second injection for L-DOPA]). It was noted, however, that while the dyskinesia was practically eliminated other behavioral abnormalities appeared to be present in the 8-OH-DPAT treated state (i.e. an abnormally flat body posture and recurring forepaw movements, resembling previous observations connected to excessive serotonergic stimulation; Jacobs, 1974). The recorded neurophysiological signals in the eight different brain regions revealed a clear shift away from the dyskinetic state in both LFPs (Fig. 7B; MANOVA [ANOVA with frequency bands as dependent variables], $p<0.001$, mean distance in first canonical dimension were: Dys vs. 8-OH-DPAT = 24.3; 8-OH-DPAT vs. WAY100635 = 17.1; Dys vs. WAY100635 = 7.1 and all groups were significantly different to each other; $p<0.001$, Wilcoxon rank sum cf. Dupre et al., 2013) and in unit activity (Fig. 7C; MANOVA, $p<0.001$, mean distance in first canonical dimension were: Dys vs. 8-OH-DPAT = 10.9; 8-OH-DPAT vs. WAY100635 = 9.5; Dys vs. WAY100635 = 1.4 and all groups were significantly different to each other; $p<0.001$, Wilcoxon rank sum). However, a closer comparison to the control state revealed that certain differences remained between the 8-OH-DPAT treated state and the control condition. In particular, low frequency oscillations (delta/theta and beta) showed a deviant pattern (Fig. 7D; see Fig. 8 for corresponding spectrograms from all structures for the intact

hemisphere). These remaining differences between the 8-OH-DPAT treated state and control conditions, together with the observation that normal behavior was not fully reinstated with this drug, suggest that aspects of the motor behavior, other than those captured with the dyskinesia score are relevant for the interpretation of the electrophysiological state in this case.

Investigating drug effects in a systems level neurophysiological state space

Because pharmacological manipulations targeting 5HT_{1A} receptors clearly have the potential to reduce dyskinesia but nevertheless induce neurophysiological activity patterns that in some parts of the brain differ considerably to the control state, it would be of relevance to characterize the drug-induced state at a systems level. More generally, condensed systems level descriptions could conceivably offer a more straightforward way to compare complex brain states following interventions that involve diverse changes in different parts of the CNS and in different neurotransmitter systems. Thus, to test the potential of the developed technology for the experimental evaluation of drug candidates and other novel therapeutic interventions we next characterized brain states, based on LFPs recorded in the eight structures in the same animal, following treatment with 8-OH-DPAT and three other drugs with putative anti-dyskinetic effects – amantadine, levetiracetam and diazepam (Pourcher et al., 1989; Pahwa et al., 2006; Stathis et al., 2011). In parallel, behavioral assessments of the reduction of dyskinesia was quantified for all four drugs. The drugs were administered systemically to reach maximum effect at the time point of peak dyskinesia (where the animals displayed severe dyskinesia corresponding to 79±4% of the maximum compound dyskinesia score). The alleviation of dyskinetic symptoms differed between the drugs ($p<0.001$, Kruskal Wallis; ranging from no detectable effect for levetiracetam (Wolz et al., 2010) to clear alleviation of symptoms for e.g. 8-OH-DPAT) and in some cases the effect also varied either

during or across experiments. In specific, following diazepam treatment intermittent periods of AIMs were present even though dyskinesia was otherwise almost completely abolished, and in the case of amantadine the alleviation of dyskinesia was relatively weaker in one of the two experiments performed (Fig. 9A).

To get an overview of the entire data set, LFP data from six recordings (one experiment was excluded due to poor recording quality) were first represented in a common principal component (PC) space spanned by the first three PCs. Remarkably, unique and clearly separable clusters were found for each of the drugs even in this low-dimensional representation (Fig. 9B; for details on calculations see Methods). The state separation was quantified with a classifier with eight states that achieved near-perfect classification performance (>99.9%) using 30 PCs (Fig. 10). This tight clustering of neurophysiological states induced by the same treatment in separate experiments performed weeks apart clearly indicates that the drug-induced systems level states were specific and robust.

To further clarify to what extent activity patterns in different brain structures contributed to the combined state description we next analyzed how well the different drug-induced states could be separated using only a subset of the recorded structures. Hence, the classification performance of the eight states shown in Fig. 9B was calculated for all 255 possible combinations of structures (Fig. 9C). As expected, a higher number of brain structures generally improved classification performance. It was also noted that although motor cortex and STN together turned out to be the most informative pair, different combinations of structures resulted in the most accurate state classification depending on the total number included because the fraction of shared (redundant) information in a given structure will depend on which other structures that are included.

To compare the contribution from specific frequency bands we analyzed how well the states could be separated using only the theta band (3-9 Hz), only the beta band (10-35 Hz), only the

gamma band (65-100 Hz), or any combination with two or three of these bands. To make the comparison fair we used PCA to reduce the dimensionality to 8 in all test cases before classifying. The classification performances were: theta=24%, beta=20%, gamma=25%, theta+beta=22%, theta+gamma=35%, beta+gamma=29%, theta+beta+gamma=32%. This should be compared to the classification performance of 96% obtained when using the full spectrum (when also reduced to 8 PCs).

Having confirmed that each drug-induced state could be reliably identified based on multi-structure LFP data, we wanted to plot the different states using the same 2D space as in Fig. 3A to facilitate the comparison to the two pathological states that the pharmacological interventions were aimed to alleviate (i.e. PD and dyskinesia). To enable us to pool data from different subjects despite potential inter-individual differences the parkinsonian and dyskinetic states were used as reference states defining the sub-space onto which other states were then projected (the robustness of this approach was initially verified in a control experiment by training a PD/dyskinesia/amantadine classifier in one rat and cross-validating it in another rat with or without calibration to the PD and dyskinesia reference states; see Fig. 11).

In this sub-space, spanned by the basis vectors [Control vs. PD] and [Control vs. Dyskinesia]_{Ortho}, the state induced by each drug was plotted separately (Fig. 9D). In agreement with the results from the 8-OH-DPAT experiments, it is clear that while several of the drugs produced reductions of dyskinetic symptoms (as shown in Fig. 9A) the neurophysiological state was nevertheless not fully normalized and in many cases partly reverted towards the PD-state. In this context it deserves mentioning that although dyskinetic symptoms were clearly reduced by some of the drugs other aspects of the motor behavior appeared somewhat abnormal (amantadine: poor hindlimb to forelimb coordination, arching of back, postural deficits; levetiracetam: very minor reduction in

dyskinesia, flat body position; diazepam: mostly immobile but dyskinetic in association with movements).

DISCUSSION

Experimental treatment of CNS disease is conventionally evaluated in animals by documentation of changes in behavior. This approach has however a number of drawbacks. First, assessments of motor behavior only gives indirect information on the underlying brain states that the therapy aim to treat, making it almost impossible to deduce the specific pharmacological/neurophysiological effects of the treatment. Second, the sensitivity and robustness in assessments of animal behavioral are usually not sufficient to allow for differentiation between several related CNS states. Third, unbiased measures based on automated procedures are still rare making the testing procedures highly dependent on proper training of skilled observers and reduces reproducibility between labs.

Ever since the first electrophysiological measurements were carried out in awake subjects it has been known that the electrical activity of neurons frequently tend to synchronize into rhythmic patterns that vary depending on the state of the brain (Berger, 1929). The results presented in the current study confirm previous findings suggesting an association between LFP oscillations within certain frequency intervals in specific regions of the cortico-basal ganglia thalamic circuit and various motor symptoms in PD (Hammond et al., 2007; de Hemptinne et al., 2015). More importantly however, through the use of the developed techniques previous findings can now be complemented with significantly more elaborate state characterizations based on large-scale multi-structure recordings. The added value of these large-scale multi-structure recordings were tested quantitatively by comparisons against the same recordings where state classifications were based on information obtained from fewer structures, showing a higher classification performance with higher

number of structures (Fig. 9C). Similarly, we show that using the entire spectral contents in LFP-recordings rather than the power in a few pre-selected frequency bands greatly improves state classification. It should also be noted that, by aligning the assessed systems level states in each individual to a number of reference states inter-individual differences in activity patterns associated with each state is compensated for, which makes it possible to pool data across subjects without *ad hoc* re-alignment of data (this is a well-known problem in, for example, comparisons of spectral LFP-contents between parkinsonian subjects (Kühn et al., 2009)). In particular, in practical applications where for example therapeutic effects of a drug are evaluated and disease mechanisms are not of primary concern this approach can be beneficial.

Using the developed method, we have here shown that robust and detailed representations of the pathophysiological conditions associated with motor symptoms in a rodent model of PD can be attained. In addition, the complex and diverse effects of a number of different pharmacological interventions aimed at treating motor symptoms could also be characterized on a systems level. It may be worth noting in this context, that while a representation based on the systems level electrophysiological differences between the parkinsonian, dyskinetic and control states is a natural starting point for the investigation of anti-dyskinetic interventions, adding other reference states/conditions to the analyses (e.g. information about the behavioral state, the effects of other drugs etc.) will further help elucidating additional features of each state. Also, for pairwise comparisons of states such as direct comparison of the effects of two different drugs, difference spectra is a natural starting point for further analyses. In any case, the very rich data-sets obtained with the described method potentially open up for a much more exploratory/data-driven approach which can be very beneficial in this field of research due to the extreme complexity of the systems studied (Finkbeiner et al., 2015).

With regard to the animal model used in these experiments, it should be cautioned that the unilateral 6-OHDA medial forebrain bundle lesion model of PD has certain limitations. First, and most importantly, because the non-lesioned hemisphere is used as control some comparisons cannot be made in a straightforward manner between pathological and non-pathological states (for example, changes in the firing rate of individual neurons) and a certain degree of variability is inevitably inherent to the model due to differences of the exact recoding locations in different hemispheres. Second, it cannot be assumed that the physiology of the intact hemisphere in a hemi-lesioned rat is entirely comparable to that of a non-lesioned animal due to potential biological adaptations that have occurred to compensate for the lesion-induced contralateral deficits. A few examples of such physiological changes have in fact been reported (Kish et al., 1999; González-Hernández et al., 2004; Breit et al., 2008). In an attempt to estimate how large these differences are we quantitatively compared differences between intact hemispheres of lesioned and non-lesioned rats using multi-structure recordings in different animals. While not reaching significance, group differences were nevertheless confirmed (the average difference in median Euclidian distance to the non-lesioned references condition were for intact hemispheres in hemilesioned rats 140% higher than that of contralateral hemispheres in non-lesioned animals; i.e. the median distance to Group 1 for 5 vs. mean[2&4] in Fig. 12). Third, while the severe lesions used in the model is beneficial for the study of dyskinesia the limited therapeutic window for levodopa treatment precludes detailed analyses of the therapeutic effects of this drug. A strength of the unilateral model is, on the other hand, that certain factors affecting the general neurophysiological state are easier to control for in bilateral recordings with an internal control condition, such as the degree of drowsiness/alertness, periods of immobility/locomotion etc.

In relation to previous publications using 6-OHDA lesioned rats it is worth pointing out that certain differences have been observed between recordings in anesthetized preparations as compared to awake behaving animals. In particular urethane anesthetized 6-OHDA lesioned rats have been reported to display beta-oscillations with a somewhat lower oscillation frequency than awake animals (Brazhnik et al., 2014). Instead, awake rats typically display two types of beta oscillations that are dependent on the behavioral state (Avila et al., 2010; Brazhnik et al., 2014; Delaville et al., 2014). These oscillations (<15 Hz and 20-35 Hz, respectively) were indeed present also in the current study (see e.g. Fig. 2A, M1 prior to levodopa).

In addition to the presented measures, changes in functional connectivity between different structures, reflected in increased LFP-coherence and correlated spiking activity of cells in anatomically connected structures has also been implicated in the pathophysiology of PD (Hammond et al., 2007; Fuentes et al., 2010; Santana et al., 2014). Such measures have not been included in the state analyses to this point, but it is probable that the addition of pairwise coherence/correlation measures of neuronal activity within and between structures would help to further improve the performance of state classifications and would be a natural complement given the multi-structure recording design.

This methodology could also be combined with several of the recently developed techniques for genetic manipulations of neuronal sub-populations that are to date primarily performed in mice. The presented findings indicate that several brain structures should preferably be targeted. Thus, to adapt the method to a smaller brain it would be recommendable to scale down the number of electrodes used to target each brain structure in such experiments rather than reducing the number of structures.

Because motor symptoms are cardinal features of PD, neurophysiological states in parkinsonian and dyskinetic rats could here be directly matched to quantitative behavioral assessments of the displayed symptoms – essentially providing a validation of the neurophysiological read-outs for the studied conditions. Following anti-dyskinetic treatment, an apparent mismatch was sometimes observed between the reduction in dyskinesia score and the corresponding changes in systems level brain state (although the coordinate values in the dimension [Control vs Dyskinesia] indeed correlated well with dyskinesia scores, see Fig. 9 Legend). The discrepancy observed can however largely be explained by the fact that a behavioral characterization solely based on dyskinesia score does not capture a whole range of other motor symptoms that were here only described qualitatively. If more detailed behavioral assessments had been carried out with quantitative assessment scales that were adapted to include a wider range of motor symptoms it is probable that the behavioral state descriptions would be better correlated to the neurophysiological activity states recoded in these motor circuits. Notably, however, such behavioral assessments are technically very challenging to carry out and will likely require more advanced automated procedures (see e.g. Palmér et al., 2012; Santana et al., 2015). In addition, it is well known that PD also includes non-motor symptoms and in several other disorders few overt signs, if any, may be associated with a specific pathological condition. In this situation, CNS state characterizations on a more holistic level could help opening up a new window into otherwise hidden internal processes in conditions such as persistent pain states, psychosis, depression etc. We therefore envision that this technology could have an important use in the development of future treatments for a range of neurologic and psychiatric conditions. More fundamentally however, the knowledge gained from improved descriptions of how different brain structures interact to create mental states and complex behaviors in health and disease using a technology that bridges all the way from the scale of single cell activity

to systems level states has potentially wide-reaching implications for neuroscientific research in general.

ACKNOWLEDGEMENTS

The authors are thankful to Rikard Nilsson for valuable aid with histology.

GRANTS

The study was supported by grants from the Bergvall, Crafoord, Kockska, Michael J Fox, MultiPark, Olle Engkvist, Parkinson, Parkinson Research, Segerfalk, Åhlen and Åke Wiberg Foundation and from Hjärnfonden, SSMF and the VR grant [#325-2011-6441]. These sponsors had no role in study design, in the collection, analysis and interpretation of data; in the writing of the report; and in the decision to submit the article for publication. The authors declare no conflict of interest.

REFERENCES

- Alam M, Capelle H-H, Schwabe K, Krauss JK** (2013). Effect of deep brain stimulation on levodopa-induced dyskinesias and striatal oscillatory local field potentials in a rat model of Parkinson's disease. *Brain Stimul* **7**: 13–20.
- Albin RL, Young AB, Penney JB** (1989). The functional anatomy of basal ganglia disorders. *Trends Neurosci* **12**: 366–375.
- Alegre M, López-Azcárate J, Alonso-Frech F, Rodríguez-Oroz MC, Valencia M, Guridi J, et al** (2012). Subthalamic activity during diphasic dyskinesias in Parkinson's disease. *Mov Disord* **27**: 1178–1181.
- Alonso-Frech F, Zamarbide I, Alegre M, Rodríguez-Oroz MC, Guridi J, Manrique M, et al** (2006). Slow oscillatory activity and levodopa-induced dyskinesias in Parkinson's disease. *Brain* **129**: 1748–57.
- Avila I, Parr-Brownlie LC, Brazhnik E, Castañeda E, Bergstrom DA, Walters JR** (2010). Beta frequency synchronization in basal ganglia output during rest and walk in a hemiparkinsonian rat. *Exp Neurol* **221**: 307–19.
- Barthó P, Hirase H, Monconduit L, Zugaro M, Harris KD, Buzsáki G** (2004). Characterization of neocortical principal cells and interneurons by network interactions and extracellular features. *J Neurophysiol* **92**: 600–608.
- Berger H** (1929). Über das Elektroenkephalogramm des Menschen. *Arch Psychiat Nervenkr* **87**: 527–570. [In native language]

727 **Bergman H, Wichmann T, Karmon B, DeLong MR** (1994). The primate subthalamic nucleus. II.
 728 Neuronal activity in the MPTP model of parkinsonism. *J Neurophysiol* **72**: 507–520.

729 **Berke JD, Okatan M, Skurski J, Eichenbaum HB** (2004). Oscillatory entrainment of striatal neurons in
 730 freely moving rats. *Neuron* **43**: 883–896.

731 **Brazhnik E, Novikov N, McCoy AJ, Cruz A V, Walters JR** (2014). Functional correlates of exaggerated
 732 oscillatory activity in basal ganglia output in hemiparkinsonian rats. *Exp Neurol* **261**: 563–77.

733 **Breger LS, Dunnett SB, Lane EL** (2013). Comparison of rating scales used to evaluate L-DOPA-induced
 734 dyskinesia in the 6-OHDA lesioned rat. *Neurobiol Dis* **50**: 142–150.

735 **Breit S, Martin A, Lessmann L, Cerkez D, Gasser T, Schulz JB** (2008). Bilateral changes in neuronal
 736 activity of the basal ganglia in the unilateral 6-hydroxydopamine rat model. *J Neurosci Res* **86**:
 737 1388–96.

738 **Brown P** (2003). Oscillatory nature of human basal ganglia activity: relationship to the
 739 pathophysiology of Parkinson’s disease. *Mov Disord* **18**: 357–363.

740 **Brown P, Oliviero A, Mazzone P, Insola A, Tonali P, Lazzaro V Di** (2001). Dopamine dependency of
 741 oscillations between subthalamic nucleus and pallidum in Parkinson’s disease. *J Neurosci* **21**:
 742 1033–1038.

743 **Brücke C, Huebl J, Schönecker T, Neumann W-J, Yarrow K, Kupsch A, et al** (2012). Scaling of
 744 movement is related to pallidal γ oscillations in patients with dystonia. *J Neurosci* **32**: 1008–19.

745 **Cagnan H, Kuhn AA, Brown P** (2014). Co-modulation of finely tuned high-gamma band activity across
 746 hemispheres in Parkinson’s disease. *Clin Neurophysiol* **125**: 777–785.

747 **Carta M, Carlsson T, Kirik D, Björklund A** (2007). Dopamine released from 5-HT terminals is the cause
748 of L-DOPA-induced dyskinesia in parkinsonian rats. *Brain* **130**: 1819–1833.

749 **Carta M, Lindgren HS, Lundblad M, Stancampiano R, Fadda F, Cenci MA** (2006). Role of striatal L-
750 DOPA in the production of dyskinesia in 6-hydroxydopamine lesioned rats. *J Neurochem* **96**:
751 1718–27.

752 **Cassidy M, Mazzone P, Oliviero A, Insola A, Tonali P, Lazzaro V Di, et al** (2002). Movement-related
753 changes in synchronization in the human basal ganglia. *Brain* **125**: 1235–46.

754 **Chen L, Qi R, Chen XY, Xue Y, Xu R, Wei HJ** (2011). Modulation of the activity of globus pallidus by
755 dopamine D1-like receptors in parkinsonian rats. *Neuroscience* **194**: 181–188.

756 **Coppola G, Arcieri S, D'Aniello A, Messina T, Verrotti A, Signoriello G et al.** (2010). Levetiracetam in
757 submaximal subcutaneous pentylenetetrazol-induced seizures in rats. *Seizure*. Jun;19(5):296-9.

758 **Costa RM, Lin S-C, Sotnikova TD, Cyr M, Gainetdinov RR, Caron MG, et al** (2006). Rapid alterations
759 in corticostriatal ensemble coordination during acute dopamine-dependent motor dysfunction.
760 *Neuron* **52**: 359–369.

761 **Crosby NJ, Deane KHO, Clarke CE** (2003). Amantadine for dyskinesia in Parkinson's disease. *Cochrane*
762 *Database Syst Rev*

763 **Delaville C, Cruz A V, McCoy AJ, Brazhnik E, Avila I, Novikov N, Walters JR** (2014). Oscillatory Activity
764 in Basal Ganglia and Motor Cortex in an Awake Behaving Rodent Model of Parkinson's Disease.
765 *Basal Ganglia* **3**: 221–227.

766 **Duda RO, Hart PE, Stork DG** (2001). Pattern Classification. *J Classif* **24**: 654.

767 **Dupre KB, Cruz AV, Gerber CM, Eyring KW, Walters JR** (2013). High gamma cortical activity in the
768 development of L-dopa-induced dyskinesia in a rodent model of Parkinson's disease. *Soc*
769 *Neurosci* 648.01.

770 **Finkbeiner S, Frumkin M, Kassner PD** (2015). Cell-based screening: extracting meaning from complex
771 data. *Neuron* **86**: 160–74.

772 **Fuentes R, Petersson P, Siesser WB, Caron MG, Nicolelis MAL** (2009). Spinal cord stimulation
773 restores locomotion in animal models of Parkinson's disease. *Science* **323**: 1578–1582.

774 **Fuentes R, Petersson P, Nicolelis MAL** (2010). Restoration of locomotive function in Parkinson's
775 disease by spinal cord stimulation: mechanistic approach. *Eur J Neurosci* **32**: 1100–1108.

776 **Gage GJ, Stoetzner CR, Wiltschko AB, Berke JD** (2010). Selective activation of striatal fast-spiking
777 interneurons during choice execution. *Neuron* 67: 466–479.

778 **Gervasoni D, Lin S-C, Ribeiro S, Soares ES, Pantoja J, Nicolelis MAL** (2004). Global forebrain dynamics
779 predict rat behavioral states and their transitions. *J Neurosci* **24**: 11137–47.

780 **Gilmour TP, Lieu CA, Nolt MJ, Piallat B, Deogaonkar M, Subramanian T** (2011). The effects of chronic
781 levodopa treatments on the neuronal firing properties of the subthalamic nucleus and
782 substantia nigra reticulata in hemiparkinsonian rhesus monkeys. *Exp Neurol* **228**: 53–58.

783 **Gioanni Y, Lamarche M** (1985). A reappraisal of rat motor cortex organization by intracortical
784 microstimulation. *Brain Res* 344: 49–61.

785 **Goldberg JA, Boraud T, Maraton S, Haber SN, Vaadia E, Bergman H** (2002). Enhanced synchrony
786 among primary motor cortex neurons in the 1-methyl-4-phenyl-1,2,3,6-tetrahydropyridine
787 primate model of Parkinson's disease. *J Neurosci* **22**: 4639–4653.

788 **Goldberg JA, Rokni U, Boraud T, Vaadia E, Bergman H** (2004). Spike synchronization in the
789 cortex/basal-ganglia networks of Parkinsonian primates reflects global dynamics of the local
790 field potentials. *J Neurosci* **24**: 6003–6010.

791 **González-Hernández T, Barroso-Chinea P, Rodríguez M** (2004). Response of the GABAergic and
792 dopaminergic mesostriatal projections to the lesion of the contralateral dopaminergic
793 mesostriatal pathway in the rat. *Mov Disord* **19**: 1029–1042.

794 **Graul AI** (2008). Promoting, improving and accelerating the drug development and approval
795 processes. *Drug News Perspect* **22**: 30–38.

796 **Halje P, Tamtè M, Richter U, Mohammed M, Cenci MA, Petersson P** (2012). Levodopa-induced
797 dyskinesia is strongly associated with resonant cortical oscillations. *J Neurosci* **32**: 16541–16551.

798 **Hammond C, Bergman H, Brown P** (2007). Pathological synchronization in Parkinson's disease:
799 networks, models and treatments. *Trends Neurosci* **30**: 357–364.

800 **Harris KD, Henze DA, Csicsvari J, Hirase H, Buzsaki G** (2000). Accuracy of tetrode spike separation as
801 determined by simultaneous intracellular and extracellular measurements. *J Neurophysiol* **84**:
802 401–414.

803 **Hemptinne C de, Swann NC, Ostrem JL, Ryapolova-Webb ES, San Luciano M, Galifianakis NB, et al**
804 (2015). Therapeutic deep brain stimulation reduces cortical phase-amplitude coupling in
805 Parkinson's disease. *Nat Neurosci* **18**: 779–786.

806 **Huot P, Johnston TH, Koprach JB, Fox SH, Brotchie JM** (2013). The pharmacology of L-DOPA-induced
807 dyskinesia in Parkinson's disease. *Pharmacol Rev* **65**: 171–222.

808 **Ivica N, Tamtè M, Ahmed M, Richter U, Petersson P** (2014). Design of a high-density multi-channel
809 electrode for multi-structure parallel recordings in rodents. *36th Annu Int IEEE EMBS Conf IEEE*
810 *Eng Med Biol Soc* 393–396.

811 **Jacobs BL (1974)**. Effect of two dopamine receptor blockers on a serotonin-mediated behavioral
812 syndrome in rats. *Eur J Pharmacol* **27**: 363–366.

813 **Kannari, K., Yamato, H., Shen, H., Tomiyama, M., Suda, T. and Matsunaga, M. (2001),**
814 Activation of 5-HT_{1A} but not 5-HT_{1B} receptors attenuates an increase in extracellular dopamine
815 derived from exogenously administered L-DOPA in the striatum with nigrostriatal denervation.
816 *Journal of Neurochemistry*, 76: 1346–1353.

817

818 **Kish LJ, Palmer MR, Gerhardt GA** (1999). Multiple single-unit recordings in the striatum of
819 freely moving animals: effects of apomorphine and D-amphetamine in normal and unilateral 6-
820 hydroxydopamine-lesioned rats. *Brain Res* **833**: 58–70.

821

822 **Kreiss DS, Mastropietro CW, Rawji SS, Walters JR** (1997). The response of subthalamic nucleus
823 neurons to dopamine receptor stimulation in a rodent model of Parkinson's disease. *J Neurosci*
824 **17**: 6807–6819.

825 **Lalo E, Thobois S, Sharott A, Polo G, Mertens P, Pogosyan A, et al** (2008). Patterns of bidirectional
826 communication between cortex and basal ganglia during movement in patients with Parkinson
827 disease. *J Neurosci* **28**: 3008–3016.

828 **Lehew G, Nicolelis M** (2008). State-of-the-Art Microwire Array Design for Chronic Neural Recordings
829 in Behaving Animals—Methods for Neural Ensemble Recordings. *Methods Neural Ensemble Rec*
830 1–20

831 **Levy R, Hutchison WD, Lozano AM, Dostrovsky JO** (2000). High-frequency synchronization of
832 neuronal activity in the subthalamic nucleus of parkinsonian patients with limb tremor. *J*
833 *Neurosci* **20**: 7766–7775.

834 **Mitra P, Bokil H** (Oxford University Press: Oxford ; New York, 2008). Observed brain dynamics. at
835 <<http://www.loc.gov/catdir/toc/ecip0718/2007019012.html>>

836 **Nadjar A, Gerfen CR, Bezard E** (2009). Priming for l-dopa-induced dyskinesia in Parkinson’s disease: a
837 feature inherent to the treatment or the disease? *Prog Neurobiol* **87**: 1–9.

838 **Neafsey EJ, Sievert C** (1982). A second forelimb motor area exists in rat frontal cortex. *Brain Res* **232**:
839 151–156.

840 **Nini A, Feingold A, Slovín H, Bergman H** (1995). Neurons in the globus pallidus do not show
841 correlated activity in the normal monkey, but phase-locked oscillations appear in the MPTP
842 model of parkinsonism. *J Neurophysiol* **74**: 1800–1805.

843 **Olanow W, Schapira AH, Rascol O** (2000). Continuous dopamine-receptor stimulation in early
844 Parkinson’s disease. *Trends Neurosci* **23**: S117–S126.

845 **Olesen J, Gustavsson a., Svensson M, Wittchen HU, Jönsson B** (2012). The economic cost of brain
846 disorders in Europe. *Eur J Neurol* **19**: 155–162.

847 **Pahwa R, Factor SA, Lyons KE, Ondo WG, Gronseth G, Bronte-Stewart H, et al** (2006). Practice
848 Parameter: treatment of Parkinson disease with motor fluctuations and dyskinesia (an
849 evidence-based review): report of the Quality Standards Subcommittee of the American
850 Academy of Neurology. *Neurology* **66**: 983–95.

851 **Palmér T, Tamtè M, Halje P, Enqvist O, Petersson P** (2012). A system for automated tracking of
852 motor components in neurophysiological research. *J Neurosci Methods* **205**: 334–44.

853 **Paxinos G, Watson C** (Academic Press/Elsevier: Amsterdam ; Boston ;, 2007). *The rat brain in*
854 *stereotaxic coordinates*. at <[http://www.loc.gov/catdir/enhancements/fy0745/2006937142-](http://www.loc.gov/catdir/enhancements/fy0745/2006937142-d.html)
855 [d.html](http://www.loc.gov/catdir/enhancements/fy0745/2006937142-d.html)>.

856 **PD MED Collaborative Group** (2014). Long-term effectiveness of dopamine agonists and monoamine
857 oxidase B inhibitors compared with levodopa as initial treatment for Parkinson’s disease (PD
858 MED): a large, open-label, pragmatic randomised trial. *Lancet* doi:10.1016/S0140-
859 6736(14)60683-8.

860 **Peixoto MF, Araujo NP, Silva RH, Castro JP, Fukushima DF, Faria RR et al.** (2005). Effects of gabaergic
861 drugs on reserpine-induced oral dyskinesia. *Behav Brain Res.* May 7;160(1):51-9.

862 **Pesaran B** (2008). Neural signal processing: quantitative analysis of neural activity. Short course III,
863 presented at 2008 Society for Neuroscience Annual Meeting (Mitra PP, ed). 1–12.

864 **Pourcher E, Bonnet AM, Kefalos J, Dubois B, Agid Y** (1989). Effects of etybenzatropine and diazepam
865 on levodopa-induced diphasic dyskinesias in Parkinson's disease. *Mov Disord* **4**: 195–201.

866 **Santana MB, Halje P, Simplicio H, Richter U, Freire MAM, Petersson P, et al** (2014). Spinal cord
867 stimulation alleviates motor deficits in a primate model of Parkinson disease. *Neuron* **84**: 716–
868 22.

869 **Santana M, Palmér T, Simplicio H, Fuentes R, Petersson P** (2015). Characterization of long-term
870 motor deficits in the 6-OHDA model of Parkinson's disease in the common marmoset. *Behav.*
871 *Brain Res.* (April 28, 2015). doi: 10.1016/j.bbr.2015.04.037.

872 **Sharott A, Magill PJ, Harnack D, Kupsch A, Meissner W, Brown P** (2005). Dopamine depletion
873 increases the power and coherence of beta-oscillations in the cerebral cortex and subthalamic
874 nucleus of the awake rat. *Eur J Neurosci* **21**: 1413–1422.

875 **Stathis P, Konitsiotis S, Tagaris G, Peterson D** (2011). Levetiracetam for the management of
876 levodopa-induced dyskinesias in Parkinson's disease. *Mov Disord* **26**: 264–70.

877 **Stein E, Bar-Gad I** (2013). Beta oscillations in the cortico-basal ganglia loop during parkinsonism. *Exp*
878 *Neurol* **245**: 52–59.

879 **Svenningsson P, Rosenblad C, Af Edholm Arvidsson K, Wictorin K, Keywood C, Shankar B, et al**
880 (2015). Eltoprazine counteracts l-DOPA-induced dyskinesias in Parkinson's disease: a dose-
881 finding study. *Brain*

882 **Tai C-H, Boraud T, Bezard E, Bioulac B, Gross C, Benazzouz A** (2003). Electrophysiological and
883 metabolic evidence that high-frequency stimulation of the subthalamic nucleus bridges neuronal
884 activity in the subthalamic nucleus and the substantia nigra reticulata. *FASEB J* 17: 1820–1830.

885 **Tronci E, Fidalgo C, Zianni E, Collu M, Stancampiano R, Morelli M et al.** (2014). Effect of memantine
886 on L-DOPA-induced dyskinesia in the 6-OHDA-lesioned rat model of Parkinson's disease.
887 *Neuroscience*. Apr 18;265:245-52.

888 **Wang Y, Zhang QJ, Liu J, Ali U, Gui ZH, Hui YP, et al** (2010). Noradrenergic lesion of the locus
889 coeruleus increases apomorphine-induced circling behavior and the firing activity of substantia
890 nigra pars reticulata neurons in a rat model of Parkinson's *Brain Res* disease. 1310: 189–199.

891 **Winkler C, Kirik D, Björklund A, Cenci MA** (2002). L-DOPA-induced dyskinesia in the intrastriatal 6-
892 hydroxydopamine model of parkinson's disease: relation to motor and cellular parameters of
893 nigrostriatal function. *Neurobiol Dis* 10: 165–186.

894 **West MO, Carelli RM, Pomerantz M, Cohen SM, Gardner JP, Chapin JK, et al** (1990). A region in the
895 dorsolateral striatum of the rat exhibiting single-unit correlations with specific locomotor limb
896 movements. *J Neurophysiol* 64: 1233–1246.

897 **Wolz M, Löhle M, Strecker K, Schwanebeck U, Schneider C, Reichmann H, et al** (2010).
898 Levetiracetam for levodopa-induced dyskinesia in Parkinson's disease: A randomized, double-
899 blind, placebo-controlled trial. *J Neural Transm* 117: 1279–1286.

900

901

LEGENDS

Fig. 1 Parallel recordings in eight different structures of the cortico-basal ganglia-thalamic loop in each hemisphere made possible with high-density recording arrays.

A: Microelectrode recording wires (n=128) are distributed to target relevant brain structures (circles mark positions of single 30 μ m tungsten wires; 250 μ m center-to-center spacing within groups). B: The relative arrangement of wire groups is guided by a custom made 2D-array and a 3D-aligner. Wires are electrically linked to a connector via a printed circuit board (PCB). *RFA*: rostral forelimb area, *M1*: primary motor cortex, *DLS*: dorsolateral striatum, *DMS*: dorsomedial striatum, *GP*: globus pallidus, *Th*: thalamus, *STN*: subthalamic nucleus, *SNr*: substantia nigra pars reticulata.

Fig. 2 Changes in neurophysiological activity patterns in the subthalamic nucleus and primary motor cortex with the onset of dyskinesia.

A: Top: Examples of LFP spectrograms from recordings in the subthalamic nucleus and primary motor cortex in the lesioned hemisphere during a 90-min period including a time period prior to, and following, the onset of dyskinesia (dashed line; t=0 min corresponds to time point of levodopa injection). Bottom: Close-up of the low-frequency range of the spectrograms shown in the top row (power is expressed in dB relative to the estimated pink-noise floor). B: Time-averaged spectra from 9 recordings (≥ 20 min per state and recording) for the parkinsonian period (grey: individual recordings; black: average) and the dyskinetic period (pink: individual recordings; red: average).

Fig. 3 Systems level neurophysiological states associated with parkinsonism and dyskinesia.

A: Systems level state descriptions in four rats based on LFP recordings in the cortico-basal ganglia-thalamic loop (dark blue for control, black for PD, red for dyskinesia and light blue for control with levodopa). The x-axis denotes the direction in LFP spectral space where the difference between the control condition and the parkinsonian state is the largest and the y-axis represents the largest difference between the control and dyskinetic state orthogonal to the x-axis. Note the close clustering of data points from each state (each small dot represents the state coordinate during an 8s-period and shaded clouds denote dot densities) and the great similarity of the states in separate recordings (filled triangles indicate cluster centers for the states in each recording; Animal I: n=9; Animal II: n=4; Animal III: n=1; Animal IV: n=1; classification performance were for the four animals: 0.9910, 0.9782, 1 and 1; all pairwise comparisons of cluster medians were significant, $p < 0.001$, Wilcoxon rank sum). B: The average spectral differences in the eight structures for [Control vs. PD] and [Control vs. Dyskinesia]_{ortho} over all nine recordings in Animal I. (C-D) Histograms illustrating the state separability in each structure with data from all nine recordings; (C): [Control vs. PD] and (D): [Control vs. Dyskinesia]. The distributions were obtained by projecting the data onto the one dimension represented by the spectral difference vector.

Fig. 4 Spectral state differences per structure divided by animal

The average LFP spectral difference vectors in the recorded structures for Top: [Control vs. PD], Middle: [Control vs. Dyskinesia] and Bottom: [Control + levodopa (LDA) vs. Dyskinesia] over all recordings averaged per animal. Note that the spectral difference [Control vs. Dyskinesia] is shown rather than [Control vs. Dyskinesia]_{ortho} (to illustrate the true spectral difference without orthogonality constraints). Colored dots indicate significant differences between the compared

states for the corresponding frequency bin and structure (Wilcoxon rank sum, $p < 0.05$, Bonferroni corrected for multiple tests).

Fig. 5 Histograms illustrating the state separability of all recordings shown per animal

Top: [Control vs. PD] and Bottom: [Control vs. Dyskinesia]. The distributions were obtained by projecting the data onto the one dimension represented by the spectral difference vector (for example, the vector pointing from the center of the control cluster to the PD cluster). Three of the animals were used for evaluation of electrical microstimulation in a separate set of experiments and are consequently lacking recording electrodes in that structure, Th [n=2] and GP [n=1]. Notably this missing information was largely compensated for by the parallel recordings in the other structures as indicated by the histograms in the rightmost column.

Fig. 6 State plots based on changes in neuronal firing rates

Left: Heat plots of all individual unit activities from the lesioned hemisphere during different states. Each row on the y-axis represents the activity of a unit throughout an experiment, normalized to its respective maximal firing rate (color codes denoting recording structures as in Fig. 3B). Vertical white lines indicate times of drug injections during the recording and onset of dyskinesia (based on manual behavioral scoring). Right: Systems level state descriptions based on unit activity in the cortico-basal ganglia-thalamic loop in the lesioned hemisphere. The x-axis denotes the direction in unit activity-space where the difference between the parkinsonian and dyskinetic state is the largest and the y-axis represents the largest difference between the parkinsonian and drug induced state orthogonal to the x-axis. The firing rate difference between PD and dyskinesia for units in the respective

structures were, expressed in Z-scores (median/iqr): RFA: 0.56/0.63, DMS: 0.63/1.19, DLS: 0.58/1.07, GP: 0.79/1.93, Th: 1.33/0.93, STN: 0.68/0.78. Classification performance of the three states in this 2D-projection were for the four panels: 0.9708, 0.9645, 0.8556 and 0.7641. All pairwise comparisons of cluster medians were significant, $p < 0.001$, Wilcoxon rank sum.

Fig. 7 Systemic treatment with a 5-HT_{1A} receptor agonist alleviates dyskinesia and alters the neurophysiological state.

A: Severity of dyskinesia scored during 1-min periods once every 5 min (marked by crosses). Dashed lines indicate times of drug injections (levodopa was administered twice in this experiment to reach the dyskinetic state - represented by the first two lines). B: Spectrogram from all recorded structures in the lesioned hemisphere showing the relative change in LFP spectral contents throughout an example experiment where a dyskinetic rat was treated with the 5-HT_{1A} agonist 8-OH-DPAT (0.4 mg/kg i.p. at $t = 123$ min) to reduce dyskinesia. This drug effect was subsequently reversed by treatment with the 5-HT_{1A} antagonist WAY-100,635 (0.4 mg/kg i.p. at $t = 163$ min). C: Cellular activity showed clear differences between states (color code represents deviation from the mean firing rate across all four conditions for each unit; units are ordered in rows according to the mean firing rate during the non-treated parkinsonian state and the colored boxes to the left of each unit indicates structure recording, with same color codes as in Figure 3B). D: The mean differences in LFP spectral contents between the control condition and the non-dyskinetic 8-OH-DPAT treated state shown in (B), summarized for each structure separately.

Fig. 8 LFP spectrograms from the intact hemisphere in recording with 8-OH-DPAT administration

Spectrograms from the non-lesioned hemisphere from two experiments with 8-OH-DPAT administrated as a dyskinesia reducing agent (bottom panel was recorded in parallel with the data shown in Fig. 7). Vertical lines indicate times of drug injections, effects and key events during the recording.

Fig. 9 Systems level characterizations of pharmacological interventions alleviating dyskinesia.

A: Reduction in normalized dyskinesia scores following systemic treatment in the same rat with four different drugs in seven separate recordings. Wilcoxon signed rank tests for significant effects on individual AIM scores between *pre* and *post*-treatment showed significant reductions ($p < 0.05$, after Bonferroni corrections with $n = 16$ comparisons) for OL: Amantadine 2, 8-OH-DPAT 2; FL: Amantadine 2, 8-OH-DPAT 1, Diazepam; Ax: Amantadine 2, 8-OH-DPAT 1 & 2, Diazepam. B: Overview of the corresponding systems level neurophysiological states induced by the different pharmacological interventions based on the spectral contents of recorded LFPs. Note that each drug clusters in a separate region of the illustrated space spanned by the first three PCs (classification performance with 3 PCs was 0.82, cf. Fig 10; all pairwise comparisons of cluster medians were significant, $p < 0.001$, Wilcoxon rank sum). C: Cluster classification performance shown as a function of number of brain structures included in the electrophysiological measurement (red=average value for all possible combinations of x structures; blue=best combination of x structures [the composition of the best combinations are listed for one to six structures]; classification performance when all eight structures were used reached 99.94% for the $n = 5421$ samples with eight states; this performance was significantly higher than what was attained using fewer structures except for $n = 7$ structures, $p < 0.05$, Wilcoxon signed-rank test, with Bonferroni correction for multiple comparisons). D: Representation of the systems level state induced by each of the drugs in 2D-space with axes defined by the main

spectral differences [Control vs. PD] and [Control vs. Dyskinesia]_{Ortho} Pearson correlation (R^2) between the individual AIM scores shown in 9A and mean coordinate value in the [Control vs Dyskinesia]_{Ortho} dimension of the states shown in 9D were: OL=0.729 , FL=0.777, Ax=0.621, Rot=0.566, Total=0.724.

Fig. 10 Classification performance as a function of the number of principal components utilized

The classification performance for the eight states shown in Fig. 9B, plotted as a function of the number of PCs used to represent the full space. The black line shows the performance when all eight structures are used together. The colored lines show the performance when only data from a single structure is used. The dashed line represents chance level of correctly assigning a data point to one of the eight states. In this comparison each structure was represented by the average LFP spectral contents of all electrode pairs in the structure. It can be noted that despite that the number of electrodes differed (range: 5-9) classification performance was similar using the different individual structures. As expected, classification performance was higher when combining the information in all structures. It was also confirmed that the number of PCs used ($n=30$) to compress the data prior to numerical comparisons of state separability (e.g. in Fig. 9C) was sufficiently high to avoid significant information loss (the performance curves appear to have plateaued much earlier).

Fig. 11 Robustness of state space calibration across subjects shown by cross-validation of the amantadine treated state

A classifier with three states (A Gaussian mixture model for parkinsonian, dyskinetic and dyskinesia treated with amantadine;) was trained in the subspace spanned by the parkinsonian and dyskinetic state in one animal and tested in the analogous subspace in a second animal. The concentric circles

represent the Gaussians corresponding to the three states (black=PD, red=dyskinesia, green=amantadine) that were fitted using data from the first animal only. The green crosses show the positions of the samples from the amantadine treated state from the second animal after calibration using the two reference states. The purple crosses show the positions of the same samples but without calibration. With calibration the amantadine samples from the second animal was correctly identified 85% of the time (i.e. the true positive rate), which is only a slight decrease from the 89% achieved with the samples from the first animal, i.e. the data on which the classifier was trained. The corresponding false positive rates were 7% and 3%, respectively. As a comparison, the true positive rate without calibration was 26%.

Fig. 12 Control experiment with LFP spectra of the intact hemisphere in hemi-lesioned rats are similar to LFP spectra in non-lesioned animals.

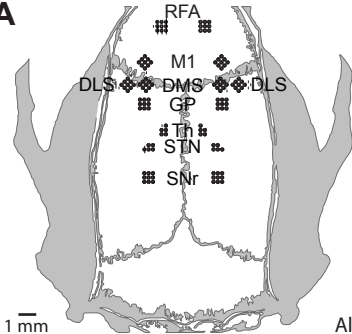
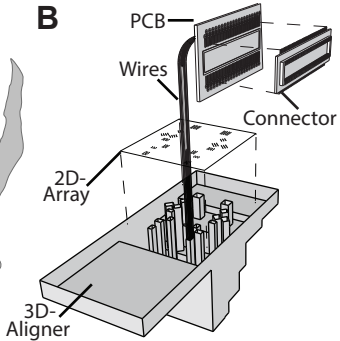
Two experiments each were conducted in four non-lesioned rats, A-D, in the following referred to as RecA₁-D₁ and RecA₂-D₂. From each of these recordings, 10 min were chosen for further analysis. The power spectral densities (PSDs) in dB_{pink} during each 10-min period were then computed for each structure as described in methods, i.e., based on 8-s windows with 50% overlap. Samples containing the concatenated spectra from all structures in one hemisphere were constructed for each such 8-s window, resulting in 149 samples each for the left and right hemisphere during the analyzed 10-min period. The same was done for a 10-min period during the off- and on-L-DOPA period, respectively, in one recording each of the hemi-lesioned rats I-IV. In summary, this resulted in the following data sets, each having a size of 149 samples x n=4; Group: 1 - Left hemispheres from RecA₁-D₁, 2 - Right hemispheres from RecA₁-D₁, 3 - Left hemispheres from RecA₂-D₂, 4 - Right hemispheres from RecA₂-D₂, 5 - Control hemispheres from hemi-lesioned rats I-IV off L-DOPA, 6 - Control hemispheres from

hemi-lesioned rats I-IV on L-DOPA, 7 – Lesioned hemispheres from hemi-lesioned rats I-IV off L-DOPA (i.e., PD state), 8 – Lesioned hemispheres from hemi-lesioned rats I-IV on L-DOPA (i.e., dyskinetic state). Displayed in this figure is the similarity of the samples in each dataset to the mean over all samples in Group 1, with the similarity being measured as the Euclidean distance of each sample to this mean. Box represents 25th to 75th percentile, i.e., the interquartile range (IQR) and red line marks median value. Whiskers mark the range for values 1.5 x IQR above or below the 75th or 25th percentile, respectively; data points outside this range are marked as outliers. Blues asterisks denote median values for individual hemispheres in each group. Significant differences between these median values on a group level were found between group 7, 8 and the control group (1; $p < 0.05$, t-test with Bonferroni correction for multiple comparisons [$n=7$]).

Table 1

A: Number of samples used. Summary of the total number of 8s samples simultaneously collected in all structures, per state (rows) and animal (columns). B: Comparison of classification performance between individual structures and all structures. Classification performance for four states (control, control + L-DOPA, PD, Dyskinesia) was evaluated for each and all structures (rows) in all animals (columns) using the 30 first PCs, and is presented in the table as the fraction of correctly classified states. Note that the best performance was always reached when all structures were utilized.

Materials, data, Matlab-code and protocols used in this publication are readily available upon request.

A**B**

A)

	Animal I	Animal II	Animal III	Animal IV
Control	4281	1661	509	434
Control + LDA	4311	1346	217	194
PD	4281	1661	509	434
Dys	4311	1346	217	194
Levetiracetam	449	-	-	-
Amantadine	1723	-	-	-
8-OH-DPAT	973	-	-	-
Way	298	-	-	-
Diazepam	749	-	-	-

B)

	Animal I	Animal II	Animal III	Animal IV
RFA	0.7242	0.5793	0.5970	0.9865
M1	0.6650	0.8387	0.6233	0.9570
DMS	0.5725	0.6875	0.6306	0.8631
DLS	0.5710	0.7220	0.5763	0.9100
GP	0.5743	0.5148	0.8957	-
Th	0.6182	-	-	0.9005
STN	0.5152	0.3755	0.6366	0.8997
SNr	0.4305	0.4487	0.7746	0.9514
All	0.9910	0.9782	1	1

